Science of the Total Environment 444 (2013) 336–346

Contents lists available at SciVerse ScienceDirect

Science of the Total Environment

journal homepage: www.elsevier.com/locate/scitotenv

A theoretical approach of absorption processes of air pollutants in sprays under droplet–droplet interaction

Wei-Hsin Chen [a,*], Shu-Mi Chen [b], Chen-I. Hung [b]

[a] Department of Greenergy, National University of Tainan, Tainan 700, Taiwan, ROC
[b] Department of Mechanical Engineering, National Cheng Kung University, Tainan 701, Taiwan, ROC

HIGHLIGHTS

- SO_2, HCl, NH_3, and HNO_3 absorbed by droplets in sprays are analyzed theoretically.
- The number density of a droplet in a spray is in the range of 10^3–10^6 cm^{-3}.
- A bubble is conceived as the sphere of influence of the droplet–droplet interaction.
- Mass diffusion number and the number density are two important factors in absorption.
- Appropriate number densities for the absorption of the four air pollutants are suggested.

ARTICLE INFO

Article history:
Received 2 October 2012
Received in revised form 23 November 2012
Accepted 3 December 2012
Available online 29 December 2012

Keywords:
Scrubbers and sprays
Droplet mutual interaction
Number density
Mass diffusion number
Scavenge wave
Sphere of influence

ABSTRACT

Sprays are an important tool for removing air pollutants through absorption. To recognize the mass transport characteristics of air pollutants in sprays, four different air pollutants of sulfur dioxide (SO_2), hydrogen chloride (HCl), ammonia (NH_3), and nitric acid (HNO_3) absorbed by droplets in sprays are analyzed theoretically in association with a numerical method. The number density of droplet in a spray is in the range of 10^3–10^6 cm^{-3} and the droplet radius is 30 μm. By conceiving a bubble as the sphere of influence of droplet–droplet interaction, the predictions indicate that the mass diffusion number and the number density are two important factors in determining the absorption process and results. When the mass diffusion number is larger, the radius of scavenging wave is increased and the effect of the droplet mutual interaction is thus intensified. An increase in number density facilitates the mass transfer of air pollutants from the gas phase to the liquid phase. However, the uptake amount of solutes by individual droplets is abated. At last, according to the mass distributions of the solutes in the liquid (droplet) phase, the appropriate number densities in sprays for the absorption of the four air pollutants are suggested.

1. Introduction

Air pollution is a noticeable environmental problem in that there is a strong relationship between air pollutants and human health (Qian et al., 2004; Makri and Stilianakis, 2008). For example, air pollutants emitted due to anthropogenic activities cause photochemical smog in the urban area, the reduction of visibility, damages on plants, human breathing difficulties, and eye irritation (Fenger, 2009). Some air pollutants will also affect the growth of vegetation and crops. For example, SO_2 and NO_x are responsible for the formation of acid rain (Percya and Ferretti, 2004) and they have harmful effects on plants, aquatic animals, and infrastructure. Acid rain also leads to soil and lake acidifications which destroy the ecosystem.

Air pollution comes from both natural processes, such as volcanoes and wildfires (Ward and Hardy, 1991), and anthropogenic activities. The main sources of air pollutants in the rural area are human-made. Power plants, chemical plants, and vehicles produce nitrogen oxides, volatile organic compounds (VOCs), carbon monoxide, carbon dioxide, sulfur dioxide, and particulates. In addition to the aforementioned air pollutants, hydrogen chloride is produced in pickling plants and plastics industry (Panda et al., 2010), and ammonia originates from industries, agriculture, and livestock breeding (Perrino et al., 2002). Nitrogen oxides are oxidized to nitric acid from combustion (Galloway et al., 1994).

To reduce air pollutant emissions, wet scrubbers have been extensively employed in industries. Wet scrubbers can be divided into six basic types: spray towers, ejector scrubbers, self-induced spray type scrubbers, rotating disk scrubbers, disintegrator scrubbers, and Venturi scrubbers (Ebert and Büttner, 1996). In the aforementioned scrubbers, the spray tower is the most commonly used one and it consists of an empty cylindrical vessel and nozzles where the aqueous absorbent is injected into the vessel from the nozzles in the form of sprays by means of fragmenting the liquid medium into droplets. The inlet gas

* Corresponding author. Tel.: +886 6 2605031; fax: +886 6 2602205.
E-mail address: weihsinchen@gmail.com (W.-H. Chen).

0048-9697/$ – see front matter © 2012 Elsevier B.V. All rights reserved.
http://dx.doi.org/10.1016/j.scitotenv.2012.12.005

Nomenclature

c	Molar concentration (M)
D	Diffusion coefficient ($m^2\ s^{-1}$)
D_m	Mass diffusion number (−)
H	Nondimensional Henry's law constant (M gas/M aqueous)
m	Nondimensional solute absorption amount
n	Number density (cm^{-3})
R	Radial coordinate (m)
t	Time (s)
u	Nondimensional concentration (−)
x	Nondimensional radial coordinate (−)
Δ	Difference

Greek letters

α	Total mass of CO_2 (−)
τ	Nondimensional time (−)

Subscript

0	Initial
b	Bubble
c	Diffusive characteristic time
d	Droplet
g	Gas phase or continuous phase
j	Grid point
l	Liquid phase or discrete phase
qss	Quasi-steady state
ss	Steady state
s	Droplet surface or interface

Superscript

p	Time step

stream usually enters the bottom of the tower and moves upward, whereas liquid is sprayed downward. Accordingly, the spray tower essentially pertains to a counter-current reactor. Simply geometry as well as low pressure drop and maintenance cost are the prime advantages of the spray tower (Bozorgi et al., 2006; Keshavarz et al., 2008).

To figure out the absorption processes in spray scrubbers, the mass transfer phenomena have been studied by a number of investigators. For example, Brogren and Karlosson (1997) analyzed the absorption process of SO_2 in a spray scrubber by using the penetration theory. Their analysis showed that the absorption process of SO_2 into the absorbent with limestone was controlled by the liquid side to a large extent. Bandyopadhyay and Biswas (2007, 2008) modeled the gaseous removal process of SO_2 in spray towers in the absence and presence of chemical reactions. The effects of the droplet size, droplet velocity, superficial gas velocity, liquid flow rate, and tower height on the performance of SO_2 scrubbing were theoretically predicted. Their results suggested that the SO_2 removal efficiency increased with the increase in the liquid flow rate, liquid-to-gas flow rate ratio, atomizing air pressure, and droplet velocity while it decreased with the increase in the droplet Sauter mean diameter and gas flow rate. Sarkar et al. (2007) developed a theoretical model by using a residence time distribution (RTD) approach to evaluate the SO_2 removal efficiency by a water spray in a horizontal co-current gas–liquid scrubber. They outlined that 75–99% of removal efficiency could be achieved in their approach.

In regard to the absorption processes of other air pollutants, Chen (2006a) developed a two-phase simulation method to predict the uptake behavior of hydrogen chloride (HCl) by moving the droplets at moderate initial Reynolds numbers in wet scrubbers. The results indicated that the larger the initial Reynolds number, the more significant the absorption rate of HCl by the droplets affected by the drag force. Gamisans et al. (2002) studied NH_3 removal by using H_2SO_4 solution in a Venturi scrubber through both experimental and numerical methods. A strong influence of liquid flow rate on the efficiency of pollutant removal was found in their study. Chen (2004) explored the scavenging mechanism of ammonia by a droplet in a convective flow. The predictions indicated that the gaseous ammonia was scavenged outward rapidly from the interface initially due to the intrinsic solute-sink role played by the droplet. When the exposure time was long, the scavenging wave progressively moved back to the droplet, stemming from the increase of the solute concentration at the interface.

Although there has been much research conducted concerning gaseous solute absorption in spray scrubbers, detailed information of air pollutant uptake by single droplets in spray scrubbers under the influence of droplet–droplet interaction is still absent so far, especially in recognizing the solute scavenging phenomena. For these reasons, the objective of this study is to develop a theoretical model in association with a numerical scheme to approach air pollutants captured by the droplets in spray scrubbers. Particular emphasis is on the effect of the droplet–droplet interaction upon the capture consequence. From the results, the suggestions of the spray operation and scrubber design from a practical perspective will be highlighted.

2. Mathematical formulation

2.1. Physical description and assumptions

Ahmadvand and Talaie (2010) have been pointed out that droplet dispersion crucially influenced the performance of gas removal in a scrubber; a good spatial dispersion of droplets led to a more uniform droplet concentration distribution and hence increased the scrubber performance. Because of this, this study focuses on four air pollutants of SO_2, HCl, NH_3, and HNO_3 individually absorbed by single droplets in scrubbers where it is assumed that droplets are uniformly cubic distributed in space and all droplets' size is identical. In other words, the assumption of the monodisperse sprays is adopted and the droplet size is represented by mean droplet radius. The assumption of the uniform droplet size has been employed in the studies of Piarah et al. (2001), Akbar and Ghiaasiaan (2004), Elperin and Fominykh (2005) and Keshavarz et al. (2008). To simplify the physical problem, the assumptions also include: (1) only physical absorption is considered (Elperin and Fominykh, 2005; Elperin et al., 2010); (2) the droplets and their surrounding are stationary and isothermal; (3) the solute uptake at the droplet surface obeys Henry's law; (4) the mass diffusion abides by Fick's law; (5) the mean droplet radius is 30 μm; and (6) the space between droplets is bubble.

The hypothesis of Bellan and Cuffel (1983) is adopted to approach the solute uptake by droplets in sprays. The entire space (i.e., the control volume) in a scrubber is partitioned into three regions: the droplets, the spheres of influence (i.e., the bubbles), and the space outside the bubbles. In the hypothesis, every single droplet in a spray is assumed to be individually surrounded by a bubble named as the sphere of influence. That is, the interaction among the droplets is restricted inside the bubbles so that the bubble surface is the interactive boundary. The extent of the droplet mutual interaction is represented by the droplet number density. When the number density is higher, the distance between droplets is shorter so that the bubble size is smaller (Chen et al., 2012). This results in a stronger droplet–droplet interaction. The physical configuration, governing equations as well as their initial, boundary, and interfacial conditions are shown in Fig. 1.

2.2. Formulations

To observe the physical phenomena in terms of dimensionless scales, a set of dimensionless parameters is defined as follows:

$$x = \frac{r}{R_d}, \tau_g = \frac{t}{R_d^2/D_g} = \frac{t}{t_{gc}}, \tau_l = \frac{t}{R_d^2/D_l} = \frac{t}{t_{lc}}, u_g = \frac{c_g(r,t)}{c_{g0}}, u_l = \frac{c_l(r,t)}{c_{g0}} H. \quad (1)$$

Substituting the above parameters into the equations shown in Fig. 1, the non-dimensional governing equations as well as the initial, boundary, and interfacial conditions are tabulated in Table 1. The dimensionless parameter $D_m(=D_l/D_gH)$ is the mass diffusion number (Chen, 2002) which represents the mass-transfer driving force ratio between the gas phase and the liquid phase. By virtue of disregarding chemical reactions, the conservation of total mass of solute in the course of absorption is taken into account (Bellan and Cuffel, 1983) and it is expressed as

$$\frac{d}{dt}\left[n\int_0^{R_d} 4\pi r^2 c_l dr + n\int_{R_d}^{R_b} 4\pi r^2 c_g r dr + \left(1 - n\frac{4}{3}\pi {R_b}^3\right) c_g\right] = 0. \quad (2)$$

In the above equation, the first, the second and the third terms designate the absorbent in the droplet, in the bubble, and the outside space of bubbles, respectively, and n is the number density, standing

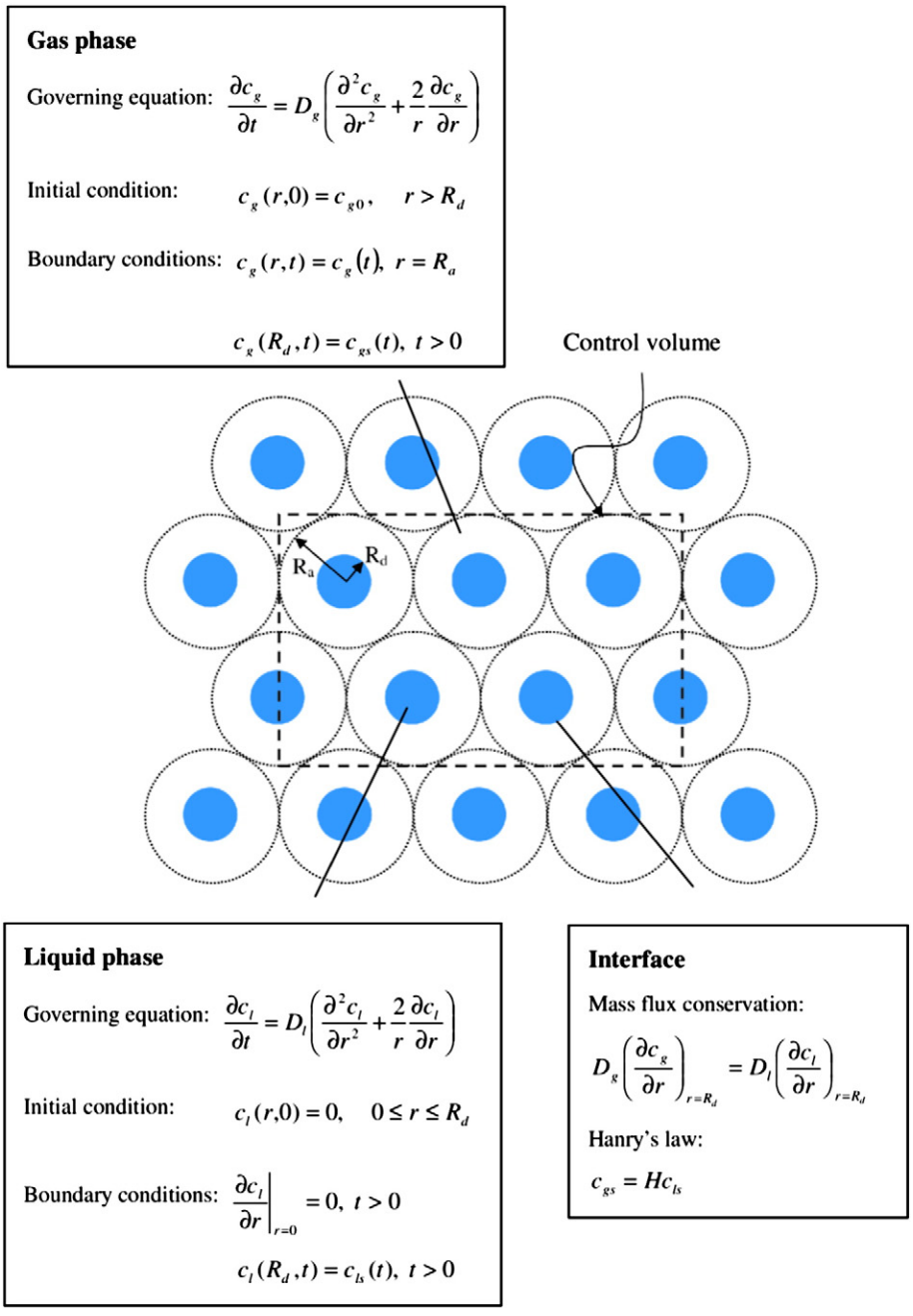

Fig. 1. A schematic of hypothesis accounting for droplet–droplet interaction in a control volume as well as the governing equations and initial, boundary, and interfacial conditions.

Table 1
A list of non-dimensional two-phase mass diffusion equations as well as boundary, initial, and interfacial conditions.

Gas phase		
Governing equation	$\frac{\partial u_g}{\partial \tau_g}=\frac{\partial^2 u_g}{\partial x^2}+\frac{2}{x}\frac{\partial u_g}{\partial x}$	(T1)
Initial condition	$u_g(x,0)=1, \quad x>1$	(T2)
Boundary conditions	$u_g\left(\frac{R_d}{R_d},\tau_g\right)=\frac{c_g(\tau_g)}{c_{g0}}$	(T3)
	$u_g(1,\tau_g)=\frac{c_{gs}}{c_{g0}}, \quad \tau_g>0$	(T4)
Liquid phase		
Governing equation	$\frac{\partial u_l}{\partial \tau_l}=\frac{\partial^2 u_l}{\partial x^2}+\frac{2}{x}\frac{\partial u_l}{\partial x}$	(T5)
Initial condition	$u_l(x,0)=0, \quad 0\le x\le 1$	(T6)
Boundary conditions	$\frac{\partial u_l}{\partial x}\mid_{x=0}=0, \quad \tau_l>0$	(T7)
	$u_l(1,\tau_l)=\frac{c_{ls}}{c_{g\infty}}H, \quad \tau_l>0$	(T8)
Interface		
Mass flux conservation	$\left(\frac{\partial u_g}{\partial x}/\frac{\partial u_l}{\partial x}\right)_{x=1}=D_m$	(T9)
Henry's law	$u_{gs}=u_{ls}$	(T10)

for the total number of droplets in a cubic centimeter (cm^{-3}). R_b is the radius of bubble (Fig. 1) and it is defined by

$$R_b=\left[0.74\frac{3}{4\pi n}\right]^{1/3}. \tag{3}$$

Physically, the total mass of the solute in a control volume remains unchanged with time, this implies

$$n\int_0^{R_d}4\pi r^2 c_l dr+n\int_{R_d}^{R_b}4\pi r^2 c_g(r)dr+\left(1-n\frac{4}{3}\pi {R_b}^3\right)c_g=\text{constant}. \tag{4}$$

Substituting the dimensionless parameters in Eq. (1) into the above equation gives

$$\frac{n}{H}\int_0^1 4\pi x^2 u_l dx+n\int_1^{\frac{R_b}{R_d}}4\pi x^2 u_g dx+\frac{1}{{R_d}^3}\left(1-n\frac{4}{3}\pi {R_b}^3\right)u_g=\alpha. \tag{5}$$

The constant α shown in Eq. (5) can be obtained from the initial conditions of Eqs. (T2) and (T6) found in Table 1 as

$$\alpha=\frac{1}{{R_d}^3}-n\frac{4\pi}{3} \tag{6}$$

When the solute uptake reaches the steady state, Eq. (5) becomes

$$\frac{n}{H}\frac{4\pi}{3}u_{l,ss}-n\frac{4\pi}{3}u_{g,ss}+\frac{1}{{R_d}^3}u_{g,ss}=\alpha. \tag{7}$$

Accordingly, the dimensionless steady-state concentrations in the gas phase and the liquid phase are obtained as

$$u_{l,ss}=u_{g,ss}=\frac{\frac{1}{{R_d}^3}-n\frac{4\pi}{3}}{\frac{n}{H}\frac{4\pi}{3}-n\frac{4\pi}{3}+\frac{1}{{R_d}^3}}. \tag{8}$$

When a solute is absorbed into a droplet, the dimensionless absorption amount of the solute in the droplet is expressed as

$$m=\frac{\int_0^{2\pi}\int_0^{\pi}\int_0^{R_d}u_l r^2\sin\theta dr d\theta d\psi}{4\pi R_d^3/3}=3\int_0^1 u_l x^2 dx. \tag{9}$$

The droplet is in saturated state if the dimensionless absorption amount is equal to unity.

2.3. Numerical method

The interfacial concentrations of the two phases, namely, Eqs. (T4) and (T8) found in Table 1, are the functions of time, and a finite difference method is thus developed to predict the physical phenomena. When discretizing the diffusion equations, i.e., Eqs. (T1) and (T5) found in Table 1, the central difference scheme is adopted, and the fully implicit scheme is utilized in treating time marching procedure for the sake of numerical stability. The discretized equations are cast into the following general form:

$$A\,u_{j-1}^{p+1}+B\,u_j^{p+1}+C\,u_{j+1}^{p+1}=D\,u_j^p \tag{10}$$

$$A=\frac{2}{\Delta x_j\left(\Delta x_j+\Delta x_{j+1}\right)}-\frac{2}{x_j\left(\Delta x_j+\Delta x_{j+1}\right)} \tag{11}$$

$$B=\frac{-2}{\Delta x_{j+1}\left(\Delta x_j+\Delta x_{j+1}\right)}-\frac{2}{\Delta x_j\left(\Delta x_j+\Delta x_{j+1}\right)}-\frac{1}{\Delta\tau} \tag{12}$$

$$C=\frac{2}{\Delta x_{j+1}\left(\Delta x_j+\Delta x_{j+1}\right)}+\frac{2}{x_j\left(\Delta x_j+\Delta x_{j+1}\right)} \tag{13}$$

$$D=-\frac{1}{\Delta\tau} \tag{14}$$

where the superscript p refers to the time increment $\Delta\tau$ and the subscript j corresponds to the space increment Δx. When the discretized equations of Eq. (10) are solved, two matrixes, with one in the gas phase and the other in the liquid phase, are encountered. The two matrixes are listed in Table 2. Regarding the grid system, 100 grids with uniform distribution in the droplet is employed; in the gas phase, the grid distribution is non-uniform and the grid number is adjusted in accordance with the investigated number density. In the current study, corresponding to the number densities of 10^3, 10^4, 10^5, and 10^6 cm^{-3}, the grid numbers in the gas phase are 1871, 869, 403 and 188, respectively. The two-phase diffusion equations, interfacial concentrations, and mass conservation equation are coupled; hence an iteration procedure is employed. During solving the equations, the Newton–Raphson scheme is applied at the interface to accelerate the numerical convergence. At present, the time step of $10^{-3}\Delta\tau_l$ is chosen for time marching. In regard to the convergent criterions, the relative errors of interfacial concentrations between two iterative steps and the total mass of solute at a specific iterative step are less than 10^{-8} and 10^{-16}, respectively. The solute

Table 2
The matrix forms of non-dimensional two-phase discretized equations.

Gas phase

$$\begin{bmatrix} B_1 & C_1 & 0 & \cdots & 0 & 0 \\ A_2 & B_2 & C_2 & \cdots & 0 & 0 \\ 0 & 0 & 0 & \cdots & 0 & 0 \\ \vdots & \vdots & \vdots & \ddots & \vdots & \vdots \\ 0 & 0 & 0 & \cdots & C_{N-2} & 0 \\ 0 & 0 & 0 & \cdots & A_{N-1} & B_{N-1} \end{bmatrix}\begin{bmatrix} u_1^{p+1} \\ u_2^{p+1} \\ u_3^{p+1} \\ \vdots \\ u_{N-2}^{p+1} \\ u_{N-1}^{p+1} \end{bmatrix}=\begin{bmatrix} \frac{-1}{\Delta\tau}u_1^p-A_1u_0^{p+1} \\ \frac{-1}{\Delta\tau}u_2^p \\ \frac{-1}{\Delta\tau}u_3^p \\ \vdots \\ \frac{-1}{\Delta\tau}u_{N-2}^p \\ \frac{-1}{\Delta\tau}u_{N-1}^p-C_{N-1}u_N^{p+1} \end{bmatrix}$$

Liquid phase

$$\begin{bmatrix} A_1+B_1 & C_1 & 0 & \cdots & 0 & 0 \\ A_2 & B_2 & C_2 & \cdots & 0 & 0 \\ 0 & 0 & 0 & \cdots & 0 & 0 \\ \vdots & \vdots & \vdots & \ddots & \vdots & \vdots \\ 0 & 0 & 0 & \cdots & C_{N-2} & 0 \\ 0 & 0 & 0 & \cdots & A_{N-1} & B_{N-1} \end{bmatrix}\begin{bmatrix} u_1^{p+1} \\ u_2^{p+1} \\ u_3^{p+1} \\ \vdots \\ u_{N-2}^{p+1} \\ u_{N-1}^{p+1} \end{bmatrix}=\begin{bmatrix} \frac{-1}{\tau}u_1^p \\ \frac{-1}{\Delta\tau}u_2^p \\ \frac{-1}{\Delta\tau}u_3^p \\ \vdots \\ \frac{-1}{\Delta\tau}u_{N-2}^p \\ \frac{-1}{\Delta\tau}u_{N-1}^p-C_{N-1}u_N^{p+1} \end{bmatrix}$$

Table 3
A list of gas and liquid diffusivities, Henry's law constants, mass diffusion numbers, and the ratio of the maximum scavenging distance to the droplet radius of solutes (25 °C and 1 atm) (Reid et al., 1987; Schwartz and Freiberg, 1981; Chen, 2006b).

Parameter	SO_2	HCl	NH_3	HNO_3
D_g ($m^2\ s^{-1}$)	1.36×10^{-5}	1.89×10^{-5}	2.34×10^{-5}	1.32×10^{-5}
D_l ($m^2\ s^{-1}$)	1.8×10^{-9}	3.1×10^{-9}	2×10^{-9}	2.98×10^{-9}
$H\left(\frac{\text{mol } l^{-1} \text{ gas}}{\text{mol } l^{-1} \text{ aqueous}}\right)$	3.3×10^{-2}	2.2×10^{-3}	7.2×10^{-4}	6.1×10^{-5}
D_m	4.01×10^{-3}	7.46×10^{-2}	0.119	3.7
$\frac{R_{sw,max}}{R_d}$	3.7	13.3	18.4	39.5

uptake is assumed to reach the steady state when the relative difference of total absorption amount between two different times is less than 10^{-8}.

3. Results and discussion

Four different gases of sulfur dioxide (SO_2), hydrogen chloride (HCl), ammonia (NH_3), and nitric acid (HNO_3) individually absorbed by pure water droplets in sprays serve as the basis of the present study. The gas and liquid diffusivities, Henry's law constants, and mass diffusion numbers of the gases in pure water are tabulated in Table 3. The temperature and pressure of the control volume (Fig. 1) are 25 °C and 1 atm, respectively. Under such conditions, the studies of Adewyi and Carmichael (1982) and Gamisans et al. (2002) have suggested that the four air pollutants (SO_2, HCl, NH_3 and HNO_3) are the gas phase rather than the vapor phase. Therefore, the four air pollutants are treated as the gas phase. In reviewing past studies (Sazhin et al., 2001; Pikkula et al., 2001; Chen et al., 2002), the radius of the droplet and number density in sprays are approximately in the ranges of 6–60 μm and 8.8×10^3–3×10^6 cm^{-3}, respectively. Accordingly, the droplet radius of 30 μm is regarded and four different number densities, consisting of 10^3, 10^4, 10^5, and 10^6 cm^{-3}, are considered to account for the mutual interaction of droplets on the uptake processes. Corresponding to the aforementioned values of the number density, the bubble radii are 561, 260, 121, and 56 μm, respectively.

3.1. Scavenging wave and sphere of influence

When the four solutes are individually absorbed by droplets, scavenging waves will be induced, stemming from the larger mass diffusion numbers of the solutes (Chen, 2006b). In this study, the scavenging distance is defined as the position of a scavenging wave with $u_g = 0.99$ which is the function of absorption time. Fig. 2 demonstrates the relationship of the droplet size, the scavenging wave, and the sphere of influence (or the bubble). When scavenging waves travel in sprays, two different situations will be encountered. In Situation 1, the development of the scavenging wave is in the bubble. The impact of the droplet–droplet interaction on the absorption process will be slight and this situation appears at the conditions of solutes with small mass diffusion numbers and dilute sprays. In Situation 2, the maximum scavenging distance in a single droplet system (Chen, 2006b) is larger than the bubble. The development of the scavenging wave in a spray will be limited in the bubble, and the solute uptake process is strongly affected by the droplet–droplet interaction. This behavior will be triggered under the conditions of solutes with larger mass diffusion numbers and dense sprays.

The distributions of the ratio of the bubble radius to the maximum scavenging distance (i.e., $R_b/R_{sw,max}$) with respect to the number density are sketched in Fig. 3 where the bubble radius is obtained from Eq. (3) and the values of the ratio of the maximum scavenging distance to the droplet radius of the four solutes are listed in Table 3 (Chen, 2006b). From the figure, it can be seen that the absorption of NH_3 and HNO_3 are always under the strong influence of the droplet–droplet interaction within the investigated range of the number density. This is attributed to the ratio of $R_b/R_{sw,max}$ being less than unity. For the absorption of HCl by droplets, the droplet mutual interaction affects the mass transport significantly when the number density is as high as 10^4 cm^{-3}. SO_2 has the smallest mass diffusion number among the four solutes. Therefore, the ratio is smaller than unity only when the number density is higher than 10^5 cm^{-3}, implying that the droplet mutual interaction plays an important role in the absorption process once the number density exceeds 10^5 cm^{-3}.

3.2. Effects of number density and mass diffusion number on absorption

Temporal distributions of dimensionless concentration at the droplet surface under three different number densities (viz., $n = 10^3$, 10^4, and 10^6 cm^{-3}) are demonstrated in Fig. 4. For the case of $n = 10^3$ cm^{-3}, the steady-state concentrations of SO_2 and HCl at the gas–liquid interface (u_s) are close to 1, especially for the former which reaches unity rapidly in the initial uptake period (Fig. 4a). This means that the droplets are almost in the saturated state when the two solutes are absorbed. The steady-state concentrations of

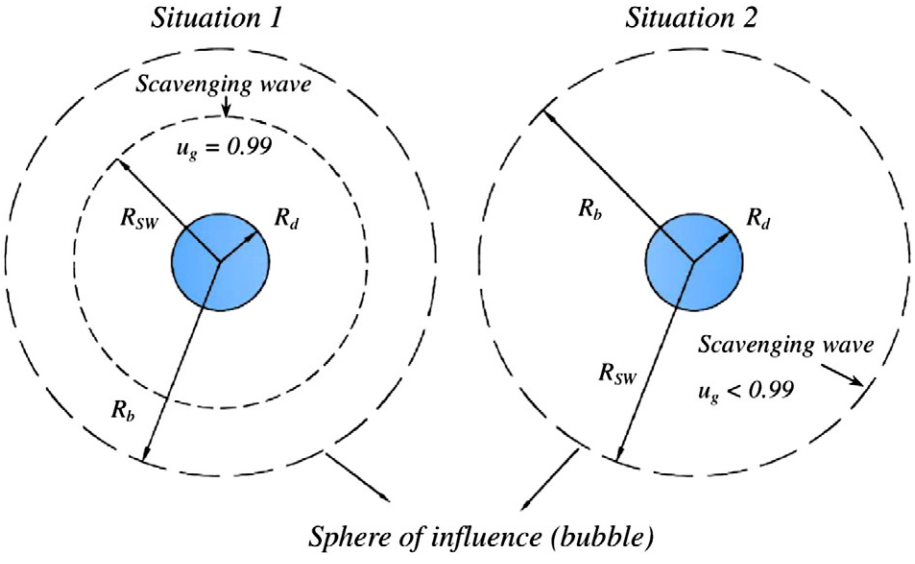

Fig. 2. A schematic of physical sizes of droplet, scavenging wave, and bubble under two different absorption situations.

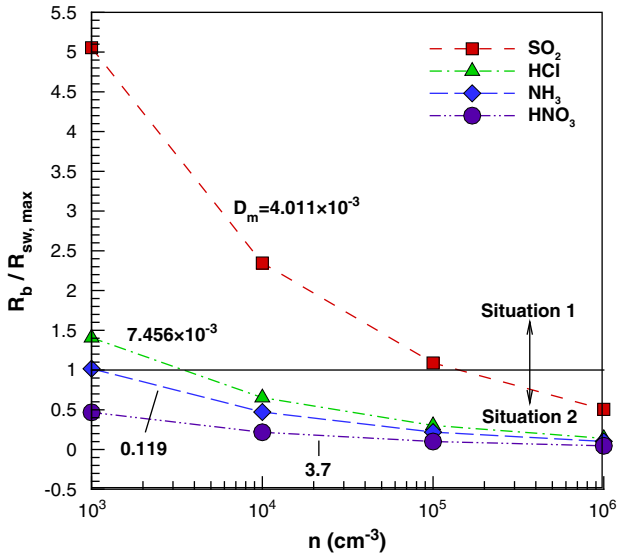

Fig. 3. Distributions of the ratio of bubble radius to the maximum scavenging distance with respect to number density.

NH_3 and HNO_3 are around 0.85 and 0.35, respectively, suggesting that 85 and 35% of the absorption capacity of the droplets are obtained. When the number density is increased to 10^4 cm^{-3}, the steady-state concentration of SO_2 is 0.97 (Fig. 4b). It follows that the droplet absorption has been affected by the droplet–droplet interaction to a small extent. In contrast, the steady-state concentration of HNO_3 is 0.05. This reflects that the droplet–droplet interaction is so pronounced that only 5% of the absorption capacity of the droplets is employed. Once the number density is as high as 10^6 cm^{-3}, the steady-state concentration of SO_2 declines to 0.2 (Fig. 4c). It is thus figured out that SO_2 absorption is also substantially affected by the droplet–droplet interaction. The steady-state concentrations of HCl, NH_3, and HNO_3 at $n=10^6$ cm^{-3} are less than 0.03. In view of a very small extent of the droplet uptake, it is inappropriate to carry out HCl, NH_3, and HNO_3 absorption in sprays at the number density of 10^6 cm^{-3}.

Temporal distributions of dimensionless concentrations of the four solutes at the bubble surface (u_{bs}) under the conditions of $n=10^3$, 10^4, and 10^6 cm^{-3} are displayed in Fig. 5. The concentrations at the bubble surface decay with increasing time, stemming from the solutes absorbed inside the bubble. Increasing mass diffusion number intensifies the absorption amount of solute by the droplets in that the number is inversely proportional to the Henry's law constant (Table 3). Therefore, the higher the mass diffusion number, the lower the concentration at the bubble surface. An increase in the number density leads to more droplets in sprays and thereby lessens the bubble size. For example, the bubble radius decreases from 561 to 56 μm when the number density increases from 10^3 to 10^6 cm^{-3}. As a result, more solutes are transported into the liquid phase and the concentrations at the bubble surface drop markedly. However, from the distributions shown in Fig. 5, it should be emphasized that relatively less solute is absorbed by single droplets as the number density increases.

From Figs. 4 and 5, it has been realized that SO_2 and HNO_3 absorbed by the droplets possess the weakest and the strongest interactions among the four solutes. Therefore, the temporal distributions of dimensionless concentration of the two solutes at the bubble surface at the four different number densities are plotted in Fig. 6. As a whole, the concentration of SO_2 is sensitive to the variation of number density in that it falls to a great extent as the number density goes up (Fig. 6a). The decaying extent of HNO_3 concentration is notable when the number density varies from 10^3 to 10^4 cm^{-3} (Fig. 6b). However, once the number density is larger than 10^4 cm^{-3}, the decrement of the concentration with increasing number density is slight. For the case of $n=10^4$ cm^{-3}, the

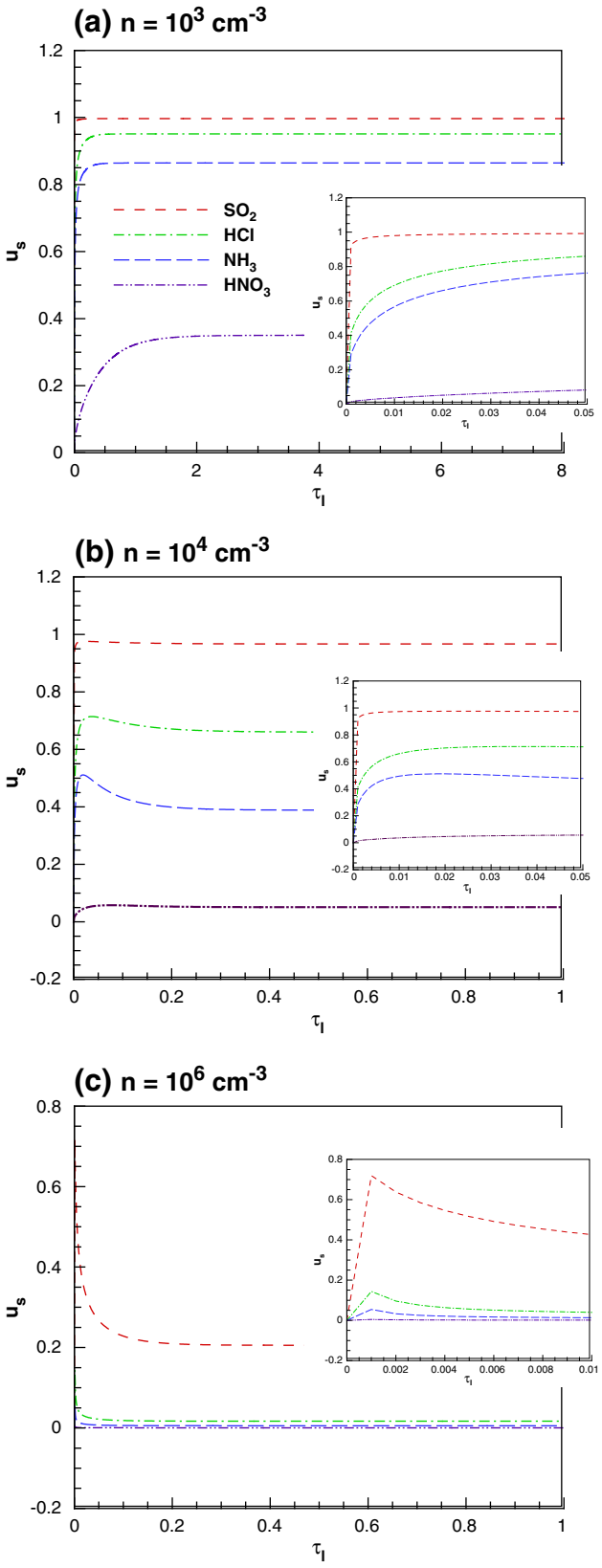

Fig. 4. Temporal distributions of dimensionless concentrations at the droplet surface under the number densities of (a) 10^3, (b) 10^4, and (c) 10^6 cm^{-3}.

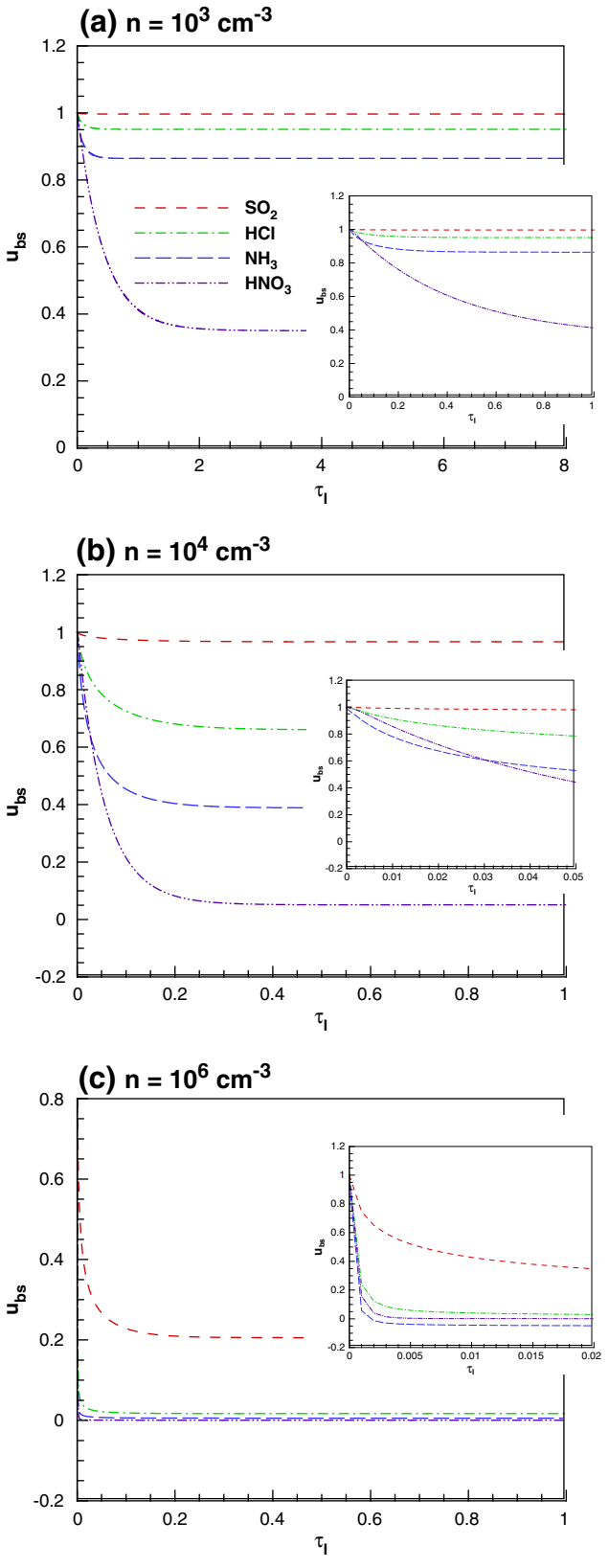

Fig. 5. Temporal distributions of dimensionless concentrations at the bubble surface under the number densities of (a) 10^3, (b) 10^4, and (c) 10^6 cm^{-3}.

steady-state concentration at the bubble surface are 0.05. It follows that around 95% of HNO_3 in the gas phase is transferred into the liquid phase.

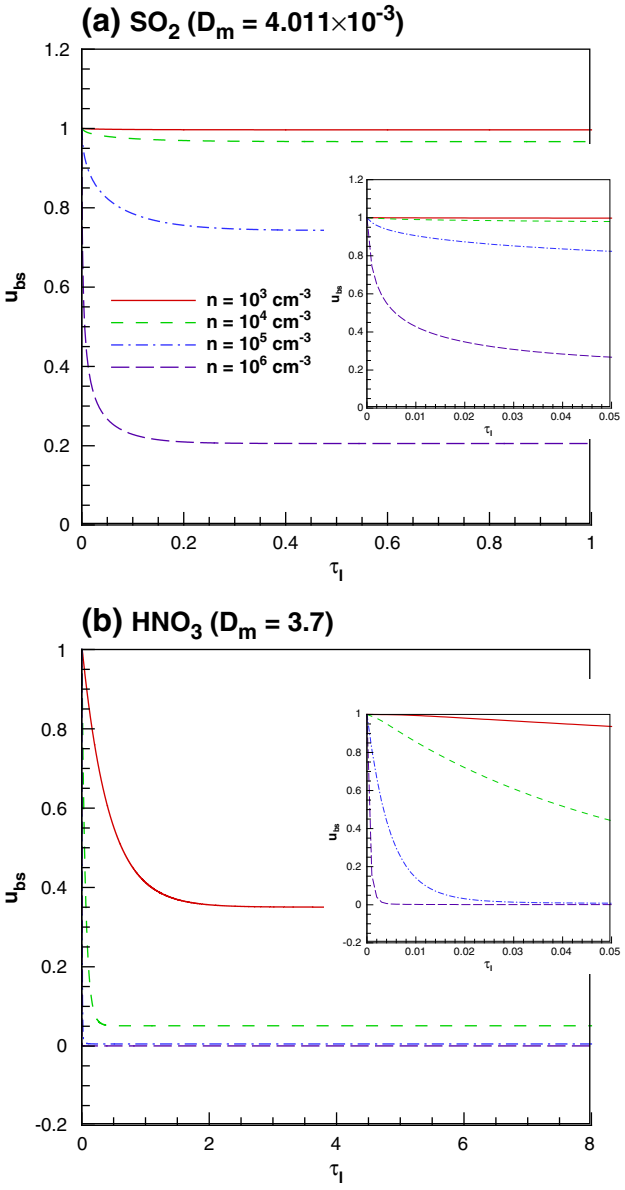

Fig. 6. Temporal distributions of dimensionless concentrations of (a) SO_2 and (b) HNO_3 at the bubble surface.

3.3. Absorption process and absorption rate

When examining the transient profile of dimensionless absorption amount (m) of SO_2 at $n = 10^3$ cm^{-3}, the solute is sufficiently absorbed by the droplets in that m approaches 1 (Fig. 7a). However, it should be mentioned that the solute concentration in the bubble is also close to 1 (Fig. 5a), revealing that most of the solute is retained in the gas phase as a consequence of the dilute spray. Increasing mass diffusion number amplifies the distance of the scavenging wave and the absorption capability of the droplets; so more solutes, say, HNO_3, are transferred into the droplet phase. However, the absorption amount of the individual droplets is reduced in that the profile is lowered. Once the number density is as high as 10^6 cm^{-3}, the profiles shown in Fig. 7b are much lower than those in Fig. 7a. This is attributed to more droplets injected in the spray; the absorption amount of individual droplets is thus reduced, no matter which solute is absorbed (Fig. 7b).

The profiles of the dimensionless quasi-steady absorption amounts (m_{qss}) and times ($\tau_{l,qss}$) as well as the absorption rates of the four

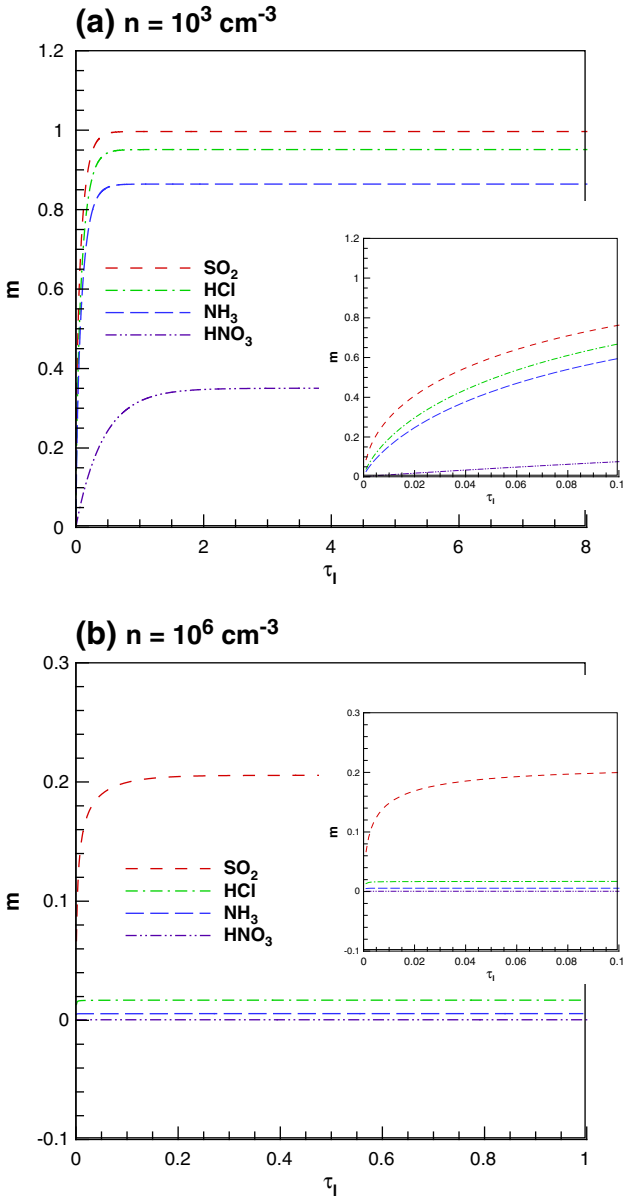

Fig. 7. Temporal distributions of dimensional absorption amount by a droplet at the number densities of (a) 10^3 and (b) 10^6 cm^{-3}.

gases are shown in Fig. 8. The quasi-steady time is identified at the moment when the absorption process reaches the state of $m_{qss} = 0.99 m_{ss}$ (Chen and Lu, 2003) and the subscript *ss* stands for the steady state. The dimensionless quasi-steady uptake amount has a trend to decrease as the mass diffusion number or the number density is lifted, indicating that the absorption capability of droplets is significantly influenced by the two factors (Fig. 8a). It is known that the absorption time plays a vital role in designing spray tower in that it determines the length of spray. The quasi-steady time is also affected by the number density; that is, the higher the number density, the lower the time is (Fig. 8b). This can be explained by the solute absorbed by more droplets so that the uptake time is shortened. When m_{qss} and $\tau_{l,qss}$ are considered together, the profiles of the dimensionless absorption rate reveal that SO_2 has the largest absorption rate, whereas HNO_3 has the smallest one. Overall, the absorption rate is the function of the mass diffusion number and the number density, except for HNO_3 which is insensitive to the number density (Fig. 8c) due to the interaction between the farther scavenging wave and the shorter droplet distance at a larger

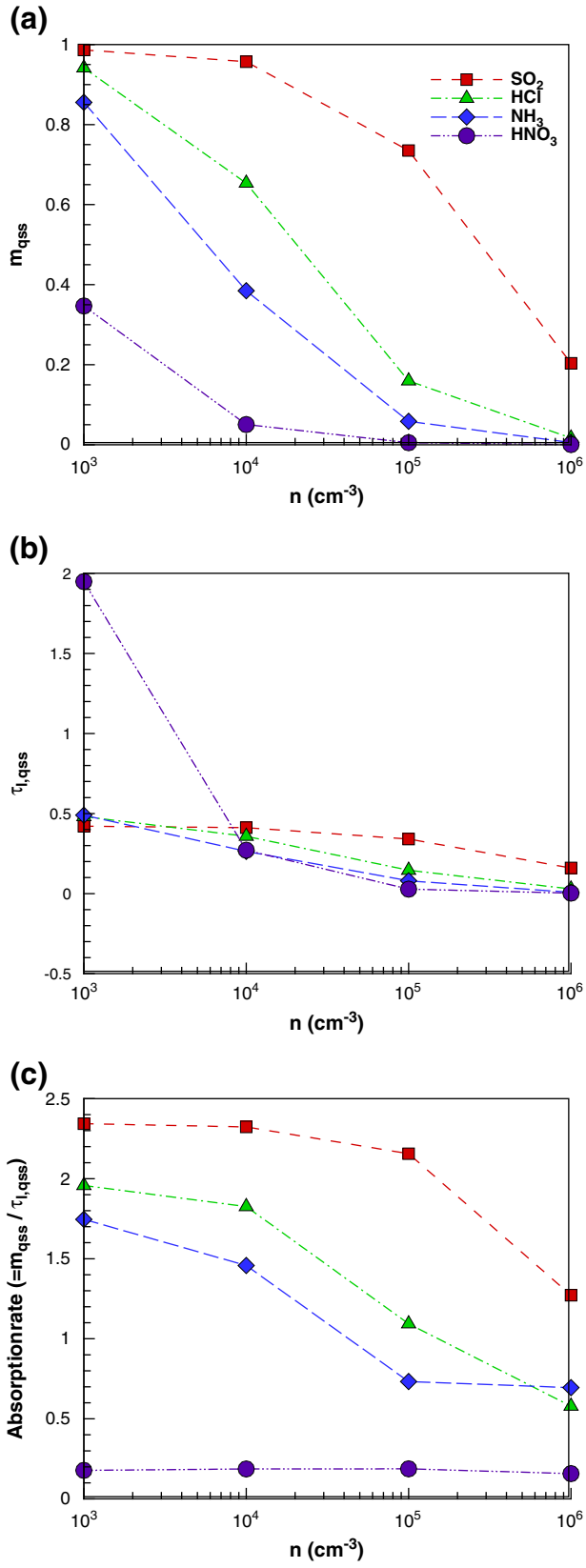

Fig. 8. Profiles of (a) quasi-steady absorption amount, (b) quasi-steady time as, and (c) absorption rate.

number density. The physical quasi-steady times (t_{qss}) of the four solutes are tabulated in Table 4. It can be seen that the value of t_{qss} for the droplets (30 μm) to absorb the solutes in sprays are less than 1 s.

Table 4
A list of quasi-steady times (s) of solutes.

Number density (cm^{-3})	SO_2	HCl	NH_3	HNO_3
10^3	0.211	0.140	0.221	0.589
10^4	0.206	0.104	0.119	0.082
10^5	0.171	0.042	0.036	0.008
10^6	0.080	0.008	0.004	0.001

3.4. Total absorption amount

Upon inspection of the mass distributions of SO_2 in droplets, bubbles, and the space outside the bubbles at $n=10^3$ cm^{-3} (Fig. 9a), most of the solute is in bubbles whereas a very little amount is in the droplets, resulting from the dilute spray. An increasing number density increases the volume of liquid phase in the scrubber; so the mass percentage of the solute in the droplets rises. From the figure, the absorption amount, the removal percentage or outlet concentration of air pollutant can be easily obtained. For instance, the removal percentage of SO_2 at $n=10^6$ cm^{-3} is around 80% (Fig. 9a). If the concentration of SO_2 in a flue gas is 1200 ppm (Slack and Holliden, 1975), after using spray scrubbing with $n=10^6$ cm^{-3} the outlet concentration of SO_2 is 240 ppm. When HCl and NH_3 are absorbed by the droplets at $n=10^5$ cm^{-3}, their mass percentages in the droplets are 84 (Fig. 9b) and 94% (Fig. 9c), respectively. Hence the condition of $n=10^5$ cm^{-3} is high enough to scavenge the two solutes in sprays. HNO_3 possesses the largest mass diffusion number among the four solutes so that near 95% of the solute is transferred into the droplets at $n=10^4$ cm^{-3}. Once the number density is as high as 10^5 cm^{-3}, all the solutes can be removed by the droplets in a scrubber.

Furthermore, the mass distributions of the four solutes in accordance to their total mass in the gas phase are presented in Fig. 10. The total mass in space (=1 L) is obtained from Eq. (4) by designating $c_l=0$ mol L^{-1} and $c_g(r)=c_g=1$ mol L^{-1} in the initial state. When the number density increases, this leads to the volume reduction of the gas phase (i.e., the space outside the droplets), and whereby the total mass of the solute is abated, especially at $n=10^6$ cm^{-3}. For both SO_2 and HCl, an increase in the number density always increases the mass percentage in the liquid phase. Unlike the preceding two solutes, when NH_3 and HNO_3 are absorbed, their maximum mass distributions in the droplets are exhibited at $n=10^5$ cm^{-3}. Once the number density is increased to 10^6 cm^{-3}, the mass percentage in the

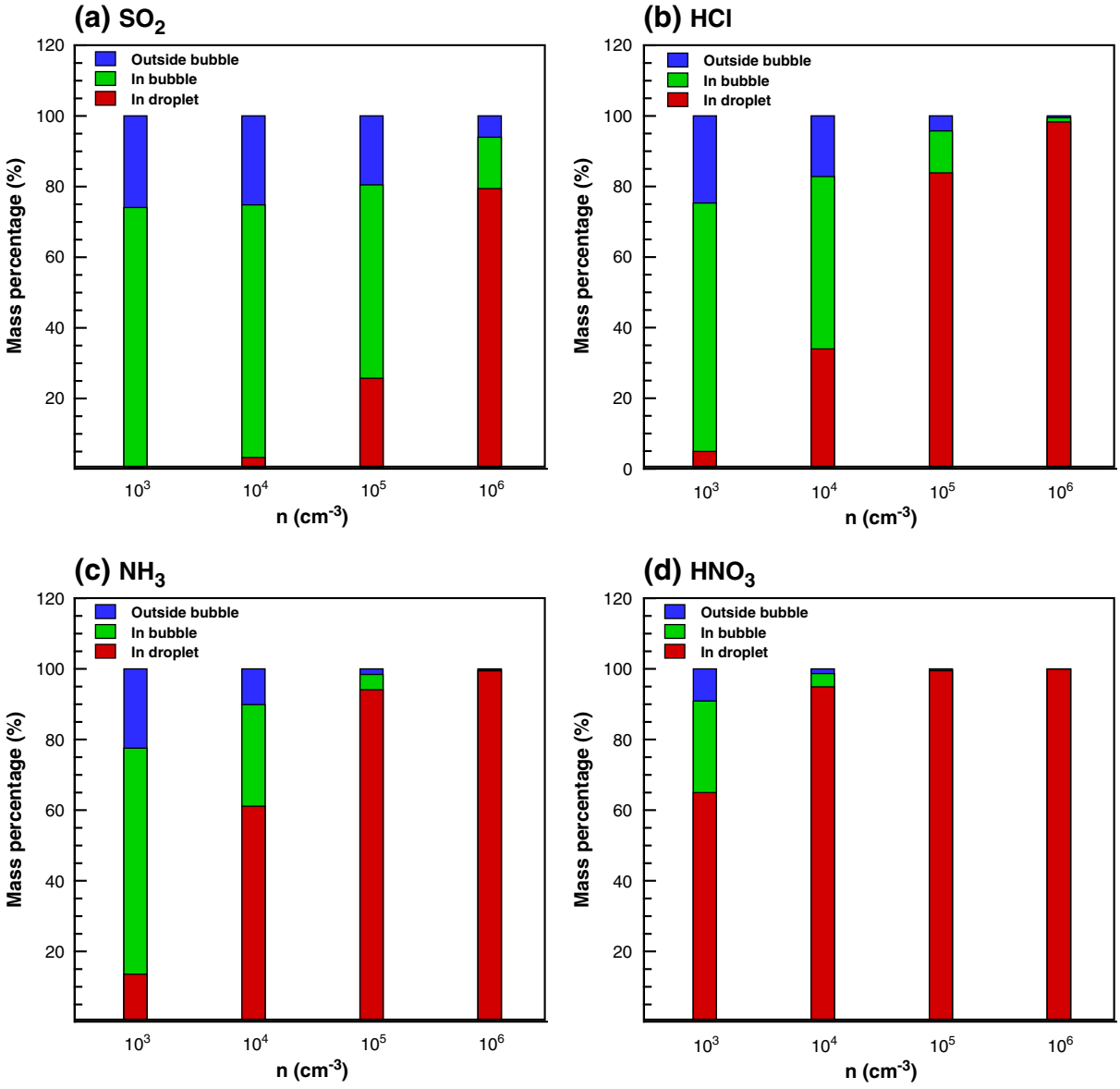

Fig. 9. Mass percentages in droplets, bubbles, and the space outside the bubbles for (a) SO_2, (b) HCl, (c) NH_3, and (d) HNO_3 in sprays.

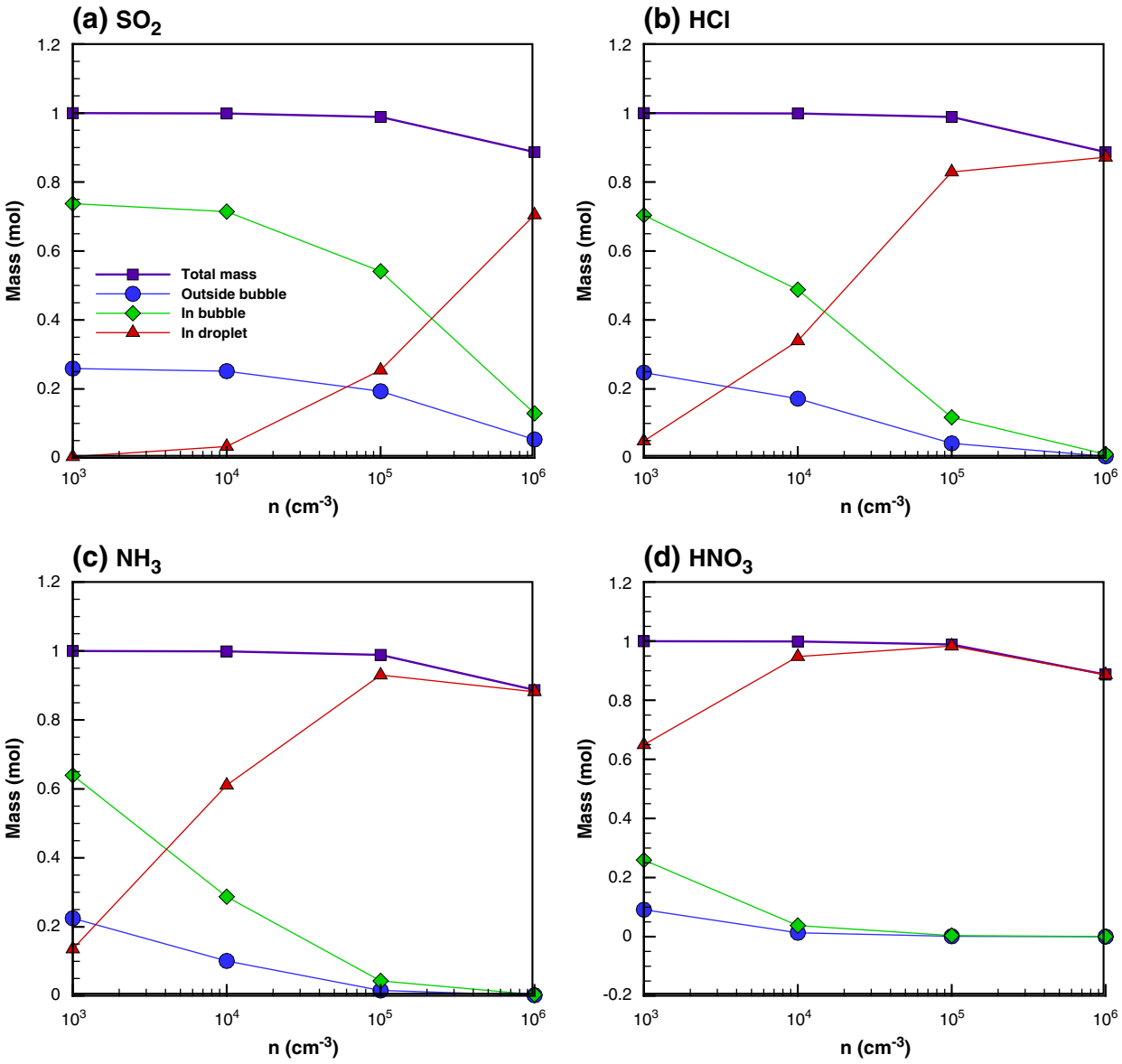

Fig. 10. Mass distributions in droplets, bubbles, and the space outside the bubbles as well as their summation for (a) SO_2, (b) HCl, (c) NH_3, and (d) HNO_3 in sprays.

droplets decreases rather than increases. This arises from the fact that relatively less solutes are in the gas phase initially. According to the profiles shown in Fig. 10, the recommended number density for the removal of SO_2 and HCl is 10^6 cm^{-3}, whereas the optimal number density to clean NH_3 and HNO_3 in the spray is 10^5 cm^{-3}.

Finally, the mass distributions of NH_3 in the droplets, bubbles and the space outside the bubbles at various mean droplet radii are demonstrated in Fig. 11 where the number density is 10^4 cm^{-3} and six different radii are considered. When the mean droplet radius is 10 μm, the mass percentage of NH_3 absorbed into the droplets is around 5.50%. Increasing the mean droplet radius significantly increases the absorption percentage. This is responsible for more water used in sprays. Once the droplet radius increases to 60 μm, the mass percentage of NH_3 in the droplets is increased to 92.69%.

4. Conclusions

A theoretical approach to account for air pollutant removal in sprays under the impact of droplet–droplet interaction has been successfully developed. In the theoretical method, the droplet mutual interaction is treated by assuming single droplets individually enveloped by spheres of influence or bubbles. The mass transport phenomena of four different solutes of SO_2, HCl, NH_3, and HNO_3 absorbed by the droplets are taken into account where the mass diffusion number is between 4.01×10^{-3} and 3.7. Meanwhile, the droplet number density in the spray ranges from 10^3 to 10^6 cm^{-3}. For a solute with a smaller mass diffusion number, say, SO_2, the maximum scavenging distance is located within the bubble when the number density is lower, and this results in a weak droplet–droplet interaction in the course of mass transfer. The absorption capacity of droplets can be sufficiently achieved; however, relatively little amount of solute is removed in sprays. An increase in mass diffusion number and number density respectively increases the maximum scavenging distance and reduces the bubble size; this intensifies the impact of the droplet mutual interaction on the solute uptake in the liquid phase. Though more solutes can be removed by spray with an increasing mass diffusion number and the number density, the absorption capability of the droplets are lowered. From a scrubber design point of view and according to the mass distributions in the gas phase and the liquid phase, the number density of 10^6 cm^{-3} is suggested to remove SO_2 and HCl, whereas 10^5 cm^{-3} is recommended for eliminating NH_3 and HNO_3 in sprays.

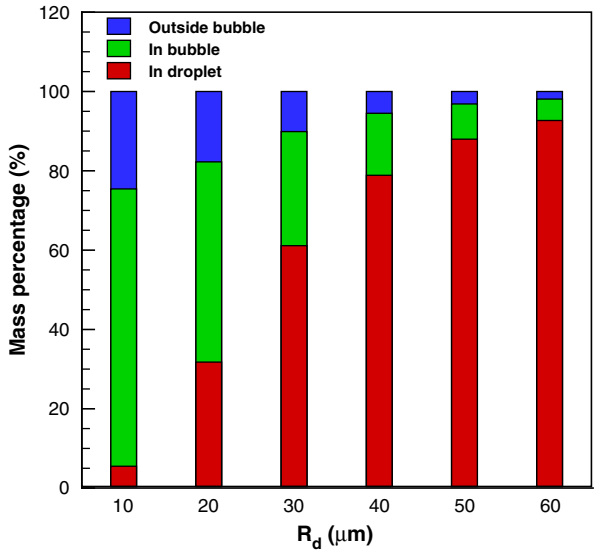

Fig. 11. Mass percentages of NH_3 in droplets, bubbles, and the space outside the bubbles at the number density of 10^4 cm^{-3} and various droplet radii.

Acknowledgments

The authors gratefully acknowledge the financial support of the National Science Council, Taiwan, ROC, for this study.

References

Adewyi YG, Carmichael GR. A theoretical investigation of gaseous absorption by water droplets from SO_2–HNO_3–NH_3–CO_2–HCl mixtures. Atmos Environ 1982;16:719–29.
Ahmadvand F, Talaie MR. CFD modeling of droplet dispersion in a Venturi scrubber. Chem Eng J 2010;160:423–31.
Akbar MK, Ghiaasiaan SM. Modeling the gas absorption in a spray scrubber with dissolving reactive particles. Chem Eng Sci 2004;59:967–76.
Bandyopadhyay A, Biswas MN. Modeling of SO_2 scrubbing in spray towers. Sci Total Environ 2007;383:25–40.
Bandyopadhyay A, Biswas MN. Critical flow atomizer in SO_2 spray scrubbing. Chem Eng J 2008;139:29–41.
Bellan J, Cuffel R. Theory of nondilute spray evaporation based upon multiple drop interactions. Combust Flame 1983;51:55–67.
Bozorgi Y, Keshavarz P, Taheri M, Fathikaljahi J. Simulation of a spray scrubber performance with Eulerian/Lagrangian approach in the aerosol removing process. J Hazard Mater 2006;B137:509–17.
Brogren C, Karlosson HT. Modeling the absorption of SO_2 in a spray scrubber using the penetration theory. Chem Eng Sci 1997;52:3085–99.
Chen WH. An analysis of gas absorption by a liquid aerosol in a stationary environment. Atmos Environ 2002;36:3671–83.
Chen WH. Atmospheric ammonia scavenging mechanisms around a liquid droplet in convective flow. Atmos Environ 2004;38:1107–16.
Chen WH. Air pollutant absorption by single moving droplets with drag force at moderate Reynolds numbers. Chem Eng Sci 2006a;61:449–58.
Chen WH. Scavenging waves and influence distances of gas absorption around single liquid aerosols in clouds. Atmos Environ 2006b;40:500–11.
Chen WH, Lu JJ. Microphysics of atmospheric carbon dioxide uptake by a cloud droplet containing a solid nucleus. J Geophys Res Atmos 2003;108(D15):4470–8.
Chen RH, Chow LC, Navedo JE. Effects of spray characteristics on critical heat flux in subcooled water spray cooling. Int J Heat Mass Transfer 2002;45:4033–43.
Chen WH, Hou YL, Hung CI. Influence of droplet mutual interaction on carbon dioxide capture process in sprays. Appl Energy 2012;92:185–93.
Ebert F, Büttner H. Recent investigations with nozzle scrubbers. Powder Technol 1996;86:31–6.
Elperin T, Fominykh A. Conjugate mass transfer during gas absorption by falling liquid droplet with internal circulation. Atmos Environ 2005;39:4575–82.
Elperin T, Fominykh A, Krasovitov B. Scavenging of soluble trace gases by falling rain droplets in inhomogeneous atmosphere. Atmos Environ 2010;44:2133–9.
Fenger J. Air pollution in the last 50 years—from local to global. Atmos Environ 2009;43:13–22.
Galloway JN, Levy HII, Kasibhatla PS. Year 2020: consequences of population growth and development on deposition of oxidized nitrogen. Ambio 1994;23(2):120–3.
Gamisans X, Sarrà M, Lafuente FJ. Gas pollutants removal in a single- and two-stage ejector–venturi scrubber. J Hazard Mater 2002;B90:251–66.
Keshavarz P, Bozorgi Y, Fathikalajahi J, Taheri M. Prediction of the spray scrubbers' performance in the gaseous and particulate scrubbing processes. Chem Eng J 2008;140:22–31.
Makri A, Stilianakis NI. Vulnerability to air pollution health effects. Int J Hyg Environ Health 2008;211:326–36.
Panda AK, Singh RK, Mishra DK. Thermolysis of waste plastics to liquid fuel: a suitable method for plastic waste management and manufacture of value added products—a world prospective. Renew Sustain Energy Rev 2010;14:233–48.
Percya KE, Ferretti M. Air pollution and forest health: toward new monitoring concepts. Environ Pollut 2004;130:113–26.
Perrino C, Catrambone M, Catrambone M, Di Bucchianico ADM, Allegrini I. Gaseous ammonia in the urban area of Rome, Italy and its relationship with traffic emissions. Atmos Environ 2002;36:5385–94.
Piarah WH, Paschedag A, Kraume M. Numerical simulation of mass transfer between a single drop and an ambient flow. Am Inst Chem Eng 2001;47:1701–4.
Pikkula BM, Torres JH, Tunnell JW, Anvari B. Cryogen spray cooling: effects of droplet size and spray density on heat removal. Lasers Surg Med 2001;28:103–12.
Qian Z, Chapman RS, Hu W, Wei F, Korn LR, Zhang J. Using air pollution based community clusters to explore air pollution health effects in children. Environ Int 2004;30:611–20.
Reid RC, Prausnitz JM, Poling BE. The properties of gases and liquids. 4th ed. New York: McGrall-Hill; 1987.
Sarkar S, Meikap BC, Chatterjee SG. Modeling of removal of sulfur dioxide from flue gases in a horizontal cocurrent gas–liquid scrubber. Chem Eng J 2007;131:263–71.
Sazhin SS, Feng G, Heikal MR, Goldfarb I, Gol'dshtein V, Kuzmenko G. Thermal ignition analysis of a monodisperse spray with radiation. Combust Flame 2001;125:684–701.
Schwartz SE, Freiberg JE. Mass-transport limitation to the rate of reaction of gases in liquid droplets: application to oxidation of SO_2 in aqueous solutions. Atmos Environ 1981;15:1129–44.
Slack AV, Holliden GA. Sulfur dioxide removal from waste gases. 2nd ed. New Jersey: Noyes Data Corporation, Park Ridge; 1975.
Ward DE, Hardy CC. Smoke emissions from wildland fires. Environ Int 1991;17:117–34.